Received 22 November 2022; revised 15 January 2023; accepted 3 February 2023. Date of publication 7 February 2023; date of current version 21 February 2023.

Digital Object Identifier 10.1109/OJAP.2023.3243408

Novel Design Methodology for 3D-Printed Lenses for Travelling Wave Antennas

AAKASH BANSAL (Member, IEEE), CHINTHANA J. PANAGAMUWA, AND WILLIAM G. WHITTOW AFWES SFHEA SMIEEE (Senior Member, IEEE)

Wolfson School of Mechanical, Electrical, and Manufacturing Engineering, Loughborough University, LE11 3TU Loughborough, U.K.

CORRESPONDING AUTHOR: A. BANSAL (e-mail: a.bansal@lboro.ac.uk).

ABSTRACT A novel methodology is introduced for designing bespoke homogeneous and graded index lenses for enhancing the gain of travelling wave antenna arrays (TWAs). 3D-printed lenses in the literature are majorly explored with standing wave antennas (SWAs) such as a microstrip or a horn antenna for gain enhancement. As there is progressively less power radiated from each slot in a TWA, as well as the successive phase delay between slots, the existing lens design approaches used for SWAs is not optimal for TWAs. Accordingly, we present a new approach of introducing a curvature to the lens that is derived from studying the power radiation profile of each slot of the TWA. This new methodology is demonstrated on a dielectric filled waveguide (DFW) slot array antenna operating at 26 – 30 GHz band. An optimized dielectric graded lens and an optimized homogeneous lens have both been designed, fabricated, and measured with the DFW slot array. The new lens demonstrated a gain enhancement of more than 7 dB compared to less than 4 dB with conventional dielectric lenses. The proposed lens theory has been further verified with a bespoke optimized lens for a periodic stub-loaded microstrip leaky-wave antenna with a beam-scanning of 65°. Design rules are included that can be applied for any TWA.

INDEX TERMS Dielectric lens, 3D-printed lens, travelling wave antenna (TWA), additive manufacturing.

I. INTRODUCTION

DIELECTRIC lenses are well-known components in antenna systems that have been used for more than a decade for beam-shaping and gain enhancement, providing highly directive antenna systems. In the literature, various dielectric lenses have been described based on transformation optics [1], wave optics [2], [3], and field transformation [4], [5].

A conventional graded flat lens (GFL) has a varying refractive index across its cross-section which enables the collimation of incident electromagnetic radiation without the need for a curvature. Graded refractive index has been achieved with different techniques such as 3D printing [2], [6], metamaterial loading over a narrow bandwidth [7], [8], [9], etc. Most studies with dielectric lenses have been described with horn antennas or similar standing wave antennas (SWAs), such as microstrip patch antennas [10], [11], [12], [13], [14], [15], [16], [17], producing gain enhancements of approximately 14 dB with two-dimensional lens structures and 7 dB with one-dimensional lens structures.

With the need for more directive beam-steering antenna systems for fifth generation mobile communications [18], [19], [20], the use of TWAs has become more popular. TWAs produce an extremely narrow beam in one plane with a wide beam in the other. A 1-D dielectric lens could be a valuable addition for such TWAs to further enhance directivity.

Conventional lenses in the literature have been used for TWAs but have a smaller gain enhancement than a similar lens when used with a SWA. A 3-D printed dielectric lens antenna was presented in [21] for improving the performance of a DFW slot array antenna for applications in 5G, and demonstrated a gain improvement of only 3 dB. A similar gain enhancement of ∼4 dB for a DFW slot array antenna was shown with the help of a metallic grating cover behaving as a phase correcting lens in [22]. Another concave-convex lens structure was demonstrated in [23] to produce a 3 dB increase in gain for a phased-array antenna. Other similar lenses have been presented with various forms of TWAs such as a leaky-wave antenna [23] and a phased array antenna [24] providing a 3 to 4.5 dB increase in antenna gain. Several other lens-based LWAs have been discussed in the literature [24], [25], [26] but they do not treat the lens as a separate entity, and hence they cannot be considered as a guide to design optimized lenses for TWAs.

Transformation optics has also been demonstrated in the literature to design bespoke lenses for different antennas [27], [28]. DFW slot array antennas have been presented with a Rotman lens [29], [30], [31], which is a reflective type of lens. Reflective type dielectric lenses are used between the feeding network and the antenna array to introduce phase delay and/or redirect the wave to specific radiating elements. Other similar reflective type lens antennas [20], [32] have been reported to operate with TWAs. Those lenses act as beamforming networks and do not have any impact on improving the antenna's directivity.

Radiating elements in a TWA are arranged in a linear sequential fashion, so each element is fed after the previous element has already radiated. Hence, unlike SWAs, radiation from each element in a TWA undergoes a series of phase delays (PD) and amplitude reductions (AR) along the length of the antenna. This continuous change affects the electrical properties of the generated wavelet, which in turn reduces the effectiveness of a conventional dielectric lens positioned in front of it.

In this paper, a detailed study of PD and AR between radiating elements of a TWA and its effect on the performance of a dielectric lens is presented with a standard DFW slot array antenna. Section II presents a comparison between the radiation characteristics for a GFL positioned in front of both a microstrip patch and an DFW slot array antenna to show the need for a different design process for dielectric lenses to make them suitable for TWAs. Section III describes the effects of PD and AR from the different radiating elements of a DFW slot array antenna on the radiated wavelet and proposes an optimized graded lens for a TWA. Section IV presents the fabricated optimized homogeneous lens (OHL) and optimized graded lens (OGL). Measured gain for two different antennas with these lenses are compared with that of a conventional plano-convex flat lens (CPFL) to verify the proposed theory. A set of design rules for optimizing a dielectric lens for any arbitrary TWA is given in Section V. These design rules are then further verified by designing and producing an optimized lens for a different antenna: a stub loaded microstrip leaky-wave antenna in Section VI. This is followed by conclusions in Section VII.

II. CONVENTIONAL GRADED LENS PERFORMANCE COMPARISON WITH A SWA AND A TWA

A. GEOMETRY OF SWA AND TWA

A conventional graded flat lens (GFL) was simulated with both a SWA and a TWA to demonstrate that these designs are not optimal for TWAs. The study used a microstrip patch antenna (representing a standard SWA) operating at 28 GHz and a dielectric filled waveguide (DFW) slot array antenna (representing a TWA) operating in the 26 – 30 GHz band. The microstrip patch antenna had a width of $w_m = 4$ mm and length, $l_m = 3.6$ mm, and was fed with a 50 Ω microstrip line (see Figure 1(a)). The DFW slot array antenna was designed using general guidelines specified in [31] and [32]. It consisted of 16 equally spaced bow-tie shaped slots of length 7.5 mm and spacing of 6 mm in two rows, with an offset of 1 mm from the center (see Figure 1(b)). The DFW slot array antenna was fed from one end and the other end was closed with a copper wall. Both the patch and the DFW slot array antennas were designed on a Taconic TLP-5 substrate ($\varepsilon_r = 2.2$, loss tangent = 0.0009, thickness, $h = 0.787$ mm).

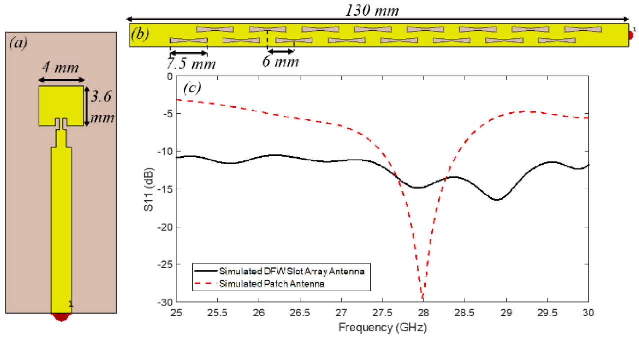

FIGURE 1. Antennas under test (a) Microstrip patch antenna representing an SWA; (b) DFW slot array antenna representing a TWA; (c) Simulated S11 for microstrip patch antenna and DFW antenna with a graded flat lens.

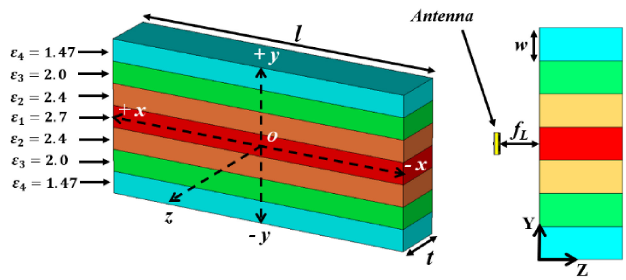

FIGURE 2. Geometry of a conventional graded flat lens (GFL) of length, l = 130 mm, thickness t = 20 mm, focal length, f_L = 10 mm and relative permittivity varying in the Y-axis from 2.7 at the center to 1.47 at the top and bottom with seven equal-width layers.

B. SIMULATED RESULTS AND DISCUSSION

Radiating elements in a TWA are arranged linearly, resulting in a wider beamwidth in the plane perpendicular to the array compared to the plane parallel to the array. Therefore, a GFL with focal length of 10 mm and a uniform relative permittivity distribution in the direction of the radiating elements was designed based on the wave optics theory described in [3]. Each layer of the lens is shown in Figure 2 and their dimensions are calculated as follows: width $w = 8$ mm and thickness $t = 20$ mm. The antenna is placed parallel to the lens at a distance equal to the focal length of 10 mm.

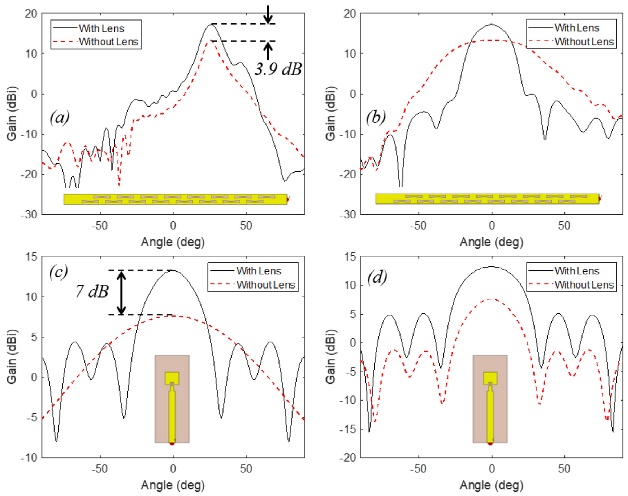

FIGURE 3. Simulated gain patterns at 28 GHz with and without GFL for DFW slot array antenna in (a) elevation and (b) azimuth planes; and for microstrip patch antenna in (c) elevation and (d) azimuth planes.

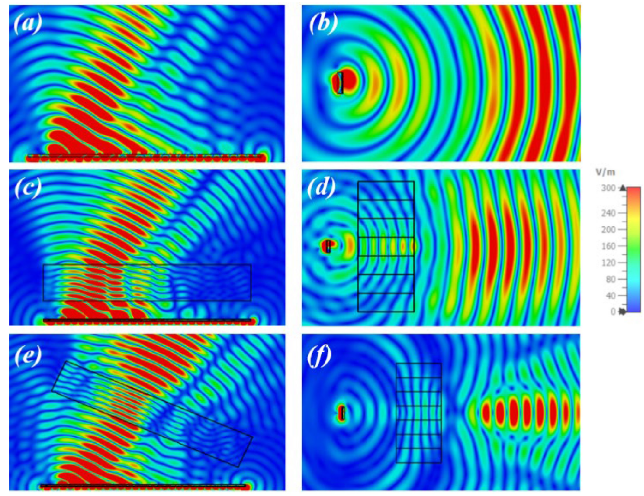

FIGURE 4. Simulated E-field plot for the DFW slot array antenna at 28 GHz (a, b) without lens, (c, d) with conventional graded flat lens (GFL) and (e, f) with tilted graded flat lens (TFL), with (a, c, e) in XZ-plane and (b, d, f) in YZ- plane.

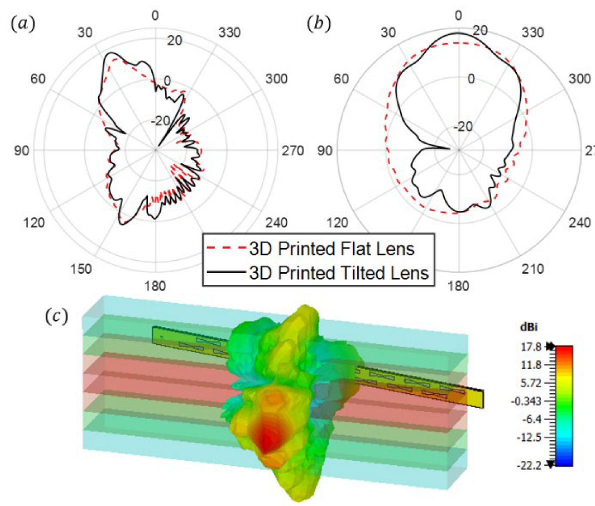

FIGURE 5. Simulated 2D gain patterns in (a) azimuth and (b) elevation planes; and (c) 3D gain pattern for a DFW slot array antenna with a TFL (where the tilt was 24°).

The length l of the lens is determined by the required focal length, size of the antenna and its beamwidth. The GFL length $l = 130$ mm was chosen to cover the full length of the DFW slot array antenna. Note, the performance of the patch antenna was the same for $l = 30$ mm and $l = 130$ mm, however, the same sized lens was used for both antennas. Simulated S11 results for both antennas mounted with lenses are given in Figure 1(c).

Figure 3 shows that the lens improved the gain of the microstrip antenna from 7.6 dBi to 14.6 dBi, demonstrating an overall increase of 7 dB. This agrees with the general improvements seen in the literature when the lens relative permittivity variation is only in one direction. However, the same lens showed an improvement of only 3.9 dB when tested with a TWA where the gain increased from 13.1 dBi to 17.0 dBi. To understand if the tilt in the beam was limiting the gain improvement, the lens was then placed perpendicular to the beam angle. Figure 3(a) shows the radiated beam is tilted by 24° at 28 GHz.

The tilt in the radiated beam is because of the travelling wave characteristics of the slot array and can be estimated using the general theory of leaky wave antennas [35], [36]. The tilt angle can be further confirmed with the simulated E-field plot for the DFW slot array antenna shown in Figure 4*(a)*. Note, a sidelobe is formed in Figure 3*(a)* at an approximate angle of 50°. This is because the radiated wavefront from the TWA is not perpendicular to the lens and hence, the transmission of the wavefront through the lens is not collimated within a single beam, leading to the formation an additional sidelobe.

When the lens is physically tilted at 24° with respect to the DFW antenna (see Figure 4(*e*)), the E-field plot shows the wavelet arriving on the lens cross-section with the same phase and hence avoiding any distortion of the overall wavelet generated by the GFL (see Figure 4(*c*)). This tilted flat lens (TFL) further improved the gain of the DFW slot array antenna by 1.2 dB compared to the GFL, but still short of the performance achieved when using the patch antenna. To confirm 24° tilt was the optimum angle for this antenna, simulations were conducted with the lens tilt angle changing from 18° to 32°. The gain was found to be highest at 24°, with a slight but acceptable reduction of 0.6 dB in antenna gain performance for a tilt from 22° to 26°.

For completeness, the E-fields in the YZ-plane for each scenario are shown in Figure 4 *(b, d, and f)*. The 2D and 3D simulated radiation patterns for the DFW slot array antenna with the tilted lens are shown in Figure 5.

Figure 4 and Figure 5 show the conventional dielectric lens is more effective for a standard SWA as compared to a TWA, even when the lens has been tilted. This difference in performance is hypothesized to be because of amplitude

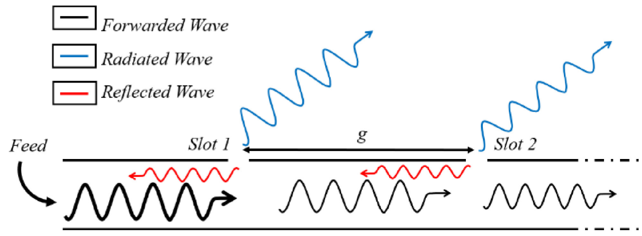

FIGURE 6. Representation of an EM wave travelling within a slotted DFW showing the radiated, reflected and forwarded waves.

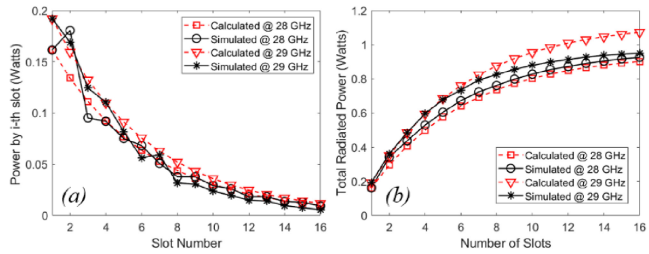

FIGURE 7. Simulated and calculated (a) power radiated by i[th] slot in 16-slot antenna; (b) total power radiated by the antenna with i-slot antenna at 28 and 29 GHz, when the antenna input power is 1W.

reduction effects that exist between the radiating elements of a TWA. It is also apparent, when titled, the focal plane of the lens is no longer coincident with the phase center of each slot. Hence, there is a need to design an optimized lens for TWAs, which is addressed in Section III.

III. OPTIMIZED DIELECTRIC LENS FOR TWA

A. EFFECTS OF AMPLITUDE REDUCTION

In this section, a DFW slot array antenna has been used to study how amplitude reduction affects the effectiveness of the lens. The design being a leaky-wave architecture on a waveguide-based guiding structure, means that it reduces leakage losses. Further, at 28 GHz DFWs are easier and cheaper to manufacture compared to standard air-filled waveguides.

The decrease in the wave amplitude in a DFW slot array antenna is illustrated in Figure 6. Neglecting all the losses within the DFW (dielectric and conductive), as the wave reaches the first slot, a fraction of the power is radiated out, some of the power is reflected and the rest continues propagating to the next slot.

To quantify the amplitude reduction, simulations were conducted for 16 different DFW slot array antennas of fixed length ($l = 130$ mm) but with different number of slots, the first antenna having only one slot and the sixteenth DFW antenna having 16 equidistant slots. Waveguide ports were defined at both ends of all the DFWs. All sixteen antennas have the same width of *5.2 mm*, height of *0.787 mm,* and relative permittivity of *2.2*.

The simulated and calculated S11 of the single slot antenna shows a good match and only 4% of the incident power is reflected. It is, therefore assumed that the reflection from the i^{th} slot has negligible effects on the $(i-1)^{th}$ slot. The power reflected, R_1, and the power continuing forward, F_1, for the single slot in the first DFW antenna can be calculated from the S11 and S21 simulated results if the input power, P_{in} is normalized to 1 W, as,

$$R_1 = |S_{11}|^2 P_{in};\ \ F_1 = |S_{21}|^2 P_{in} \tag{1}$$

The total power radiated from the first slot, P_1 can simply be calculated by subtracting from the input power P_{in} the reflected and forwarded powers. The same can be repeated for subsequent slots to calculate the power radiated by i^{th} slot, using F_{i-1} as the input power. The average relative radiated power (ARRP) by each slot, γ can be calculated as the ratio of power radiated by i^{th} slot, i.e., P_i to the power received by that slot, i.e., F_{i-1}, where F_0 is equal to the normalized power 1 W. Therefore, the ARRP can be written as,

$$\gamma = \frac{P_i}{F_{i-1}} \tag{2}$$

Using the S-Parameters from the 16 simulated antennas, the ARRP was found to be approximately constant at 17% (ranging from 16.9% to 17.2%). This means i^{th} slot on the DFW receives 83% of the power present at $(i-1)^{th}$ slot, assuming negligible losses. Hence, the power radiated by i^{th} slot can be defined as,

$$P_i = (1-\gamma)^{i-1} P_1 \tag{3}$$

This can be confirmed from Figure 7(a) and (b) which compare the simulated and calculated power radiated by individual slots and the overall antenna at 28 and 29 GHz. To incorporate the effects of this amplitude reduction on the wavelet, the TFL was further modified to follow the same logarithmic curve defined by eq. (3) and is described in detail in Sections III-B and III-C.

B. SIMULATED RESULTS FOR OPTIMIZED GRADED LENS

The optimized graded lens (OGL) was produced by implementing eq. (3) to calculate distance between lens and antenna at different points in x-axis, so that the OGL has the same curvature profile as seen in Figure 7(b). The X and Z-coordinates defining the lens curvature are given by,

$$Z(i) = -(1-\gamma)^{i-1} d \tag{4}$$

$$X(i) = l_1 + \frac{l_s}{2} + \left[g \times (n-i+1)\right] \tag{5}$$

where, i is the slot number, l_1 is the distance between the DFW feed and first slot, l_s is the slot length, n is the total number of slots and g is the distance between each slot. The parameter d is the distance from the first slot to the lens and is used to replace P_1 in eq. (3). The lens was simulated with a parametric sweep of d values between 10 and 30 mm to find the separation distance resulting in the maximum gain, and this was achieved for $d = 20$ mm.

The location of the origin O (0, 0) for X and Z is shown in Figure 8(a). The 16 points created from eq. (4) and (5) on a

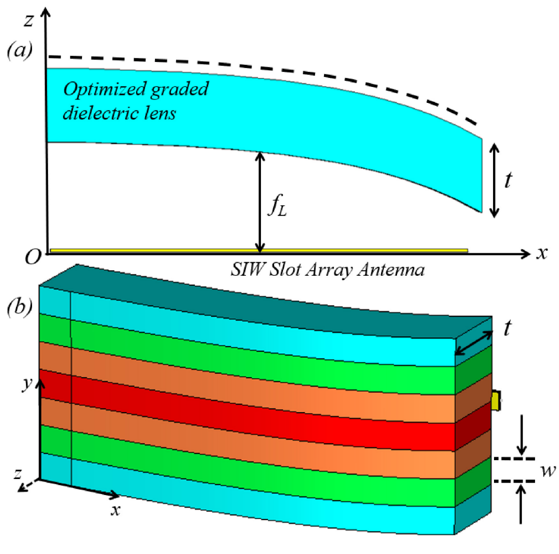

FIGURE 8. (a) Top view and (b) 3D view of the optimized graded dielectric lens (OGL) where the shape is defined by the logarithmic curve calculated by eq. (4) and (5) with the DFW slot array antenna.

TABLE 1. Simulated gain comparison for the DFW slot array antenna with different graded lens configurations.

Freq (GHz)	Gain (dBi)			
	No Lens	GFL	TFL	OGL
		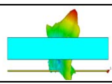	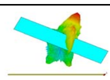	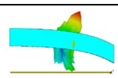
26.5	11.9	15.9	17.6	19.7
27.0	11.7	15.7	17.2	19.4
27.5	11.7	15.7	17.1	19.2
28.0	11.5	15.5	17.1	19.2
28.5	11.3	15.3	16.8	19.1
29.0	11.1	15.0	16.7	18.9
29.5	11.0	15.0	16.6	18.9

Cartesian surface with the antenna at z = 0 defines the logarithmic curvature of the lens and this cross-sectional view is shown in Figure 8 with the logarithmic curve presented as a dotted line.

With the logarithmic shape of the OGL, the antenna gain is further improved to 19.2 dBi at 28 GHz, giving an average increase of 7.6 dB compared to the gain of the DFW slot array antenna, and an average increase of 3.6 dB compared to the DFW antenna with the GFL (see Table 1).

The HPBW of the antenna system reduced from 68° without any lens to 36° with the GFL to 28° with the OGL in the elevation plane, demonstrating a significant reduction by a factor of 2.4. The 2D gain patterns demonstrating this are shown in Figure 9. The reshaping of the lens with the proposed OGL allows us to reduce the oblique incident wave from the TWA, as confirmed by the smaller side lobe levels seen in Figure 9(a). A detailed discussion on the analysis of the proposed lens design is presented in Section III-C.

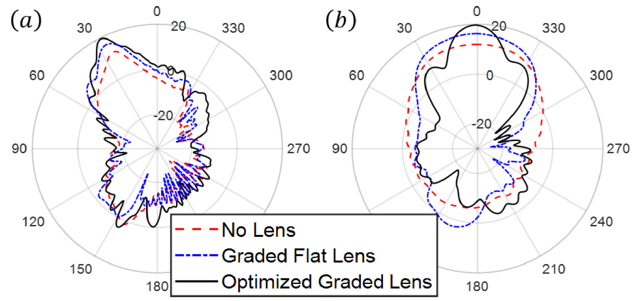

FIGURE 9. Simulated 2D gain patterns of the DFW antenna without the lens, with the graded flat lens, and with the optimized graded lens in (a) azimuth and (b) elevation planes.

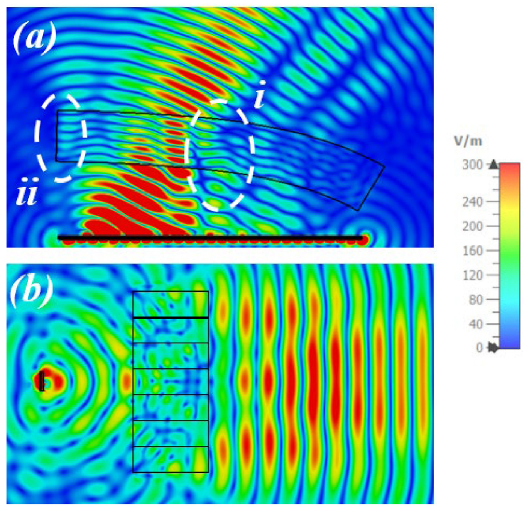

FIGURE 10. Simulated E-field plot for the DFW slot array antenna with optimized graded lens in (a) XZ plane and (b) YZ plane at 28 GHz.

C. ANALYSIS AND DISCUSSION OF OPTIMIZED LENS

The improvement in gain with the introduction of the OGL can be explained by two observations indicated in Figure 10(a). The region highlighted by '*i*' shows the radiation from the 8th slot combining with the radiation from previous slots to enhance the main beam. This phenomenon is clearly absent in the GFL in Figure 4(c) and is solely due to the curvature of the OGL. Secondly, and more importantly, region '*ii*' shows very little radiation from slot 1 missing the lens, compared to the significant wastage seen with the TFL in Figure 4(e). The curving of the OGL closer to slot 1, which radiates the most power, ensures more of the antenna's radiated power falls on the lens and so constructively contributes to the main beam. The high level of collimation seen in Figure 1(b) confirms the enhance performance of the OGL.

Due to the curving of the lens to produce the OGL, its focal line is also expected to curve. To establish its shape, a series of focal points are obtained through examining the E-field in simulations, which can be joined to form a focal line. First, the antenna is removed and the OGL is illuminated from the front with a uniform plane wave at an angle

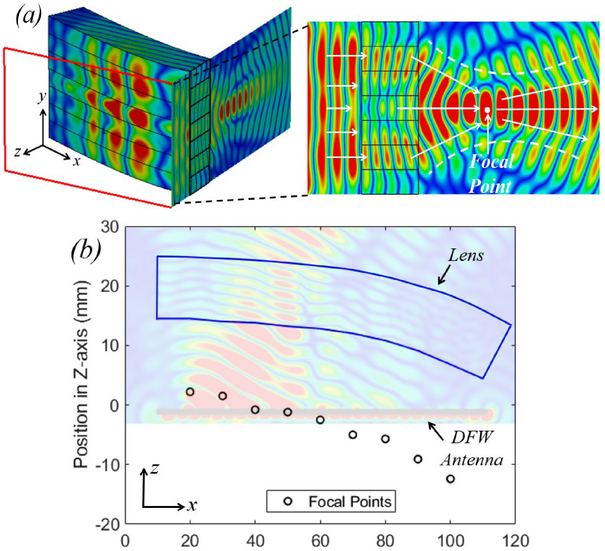

FIGURE 11. (a) Example E-field plot with the OGL cut at X = 40 mm in YZ-plane when fed with a planar wave at 28 GHz, demonstrating the focal point; (b) focal points measured from simulations at different cross-sections along the length of the lens in the X-axis.

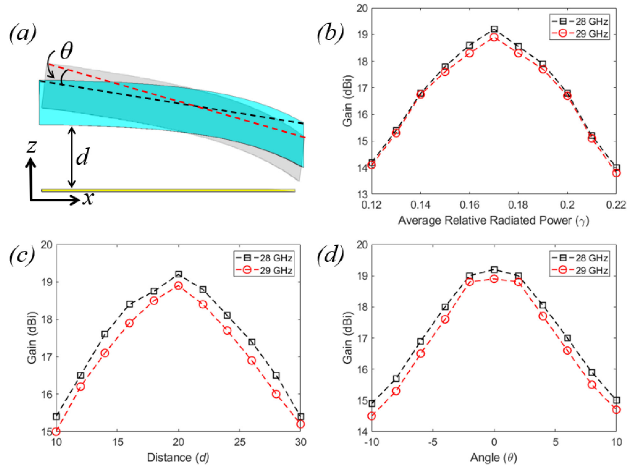

FIGURE 12. (a) Simulated OGL with antenna in XZ-plane showing change in angular tilt and distance, d; Change in gain at 28 and 29 GHz with change in (b) ARRP (affecting curvature of the lens), (c) distance between lens and antenna, and (c) tilt angle of lens.

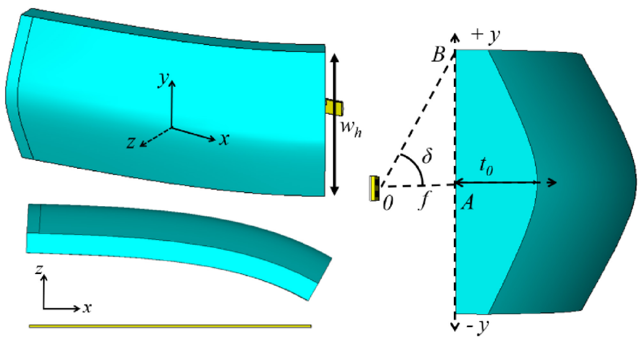

FIGURE 13. CAD model of the optimized homogeneous lens (OHL) geometry.

of 24°. The focal point distance in the YZ plane behind the lens is recorded (see Figure 11(a)) at 10 mm intervals across the length of the lens in X-axis (from 10 to 120 mm). In Figure 11(b), which is a reproduction of the E-field plot shown in Figure 10(a), the recorded focal points are superimposed. It is clear the focal line is not incident on the antenna surface. Although the radiated waves originate from the 16 slots, due to the amplitude reduction, phase delay, constructive and destructive interference, the resultant cylindrical wave appears, at least to the OGL, to originate from a virtual radiating line parallel to the wavefront, which we suggest is close to the focal line of the OGL.

To verify this was in fact the correct shape, separation distance, tilt angle for maximum gain enhancement, a parametric study was conducted. Figure 12 shows the variation in gain when the (b) curvature (relating to ARRP), (c) distance between the lens and antenna, and (d) tilt angle of the lens, are changed in simulation. It is clear the gain decreased as the design deviates from the calculated optimum parameters.

As the direction of the main beam changes with frequency, there is a small deviation in phase center. However, this only causes a minimal decrease in gain, which makes the OGL effective across the whole frequency bandwidth. We note, the focal line (composed of focal points) of the TFL would be perfectly parallel to the cylindrical wavefront, but because of its large distance from slot 1, the gain is decreased. Curving the OGL not only brings the lens closer to slot 1, but it also ensures its focal line is approximately parallel to the cylindrical wavefront. It is worth noting that the phase center of the overall antenna is at X = 40 mm in Figure 11(b), which coincidentally intersects the OGL's focal line. Furthermore, parameter d, which was optimized to be 20 mm, is also equal to the focal length of the original GFL introduced in Section II-B. This was further verified by testing the lens with different LWAs and is demonstrated in Section VI.

It is important to note that there is a slight difference between the S21 for 28 and 29 GHz, as seen in Figure 7. This should theoretically affect the shape of the lens with change in operating frequency, making the lens frequency sensitive. However, when the average relative radiated power by each slot is calculated for all the frequencies, it is 0.17 for 28 GHz and 0.16 for 29 GHz, and hence, the relative difference is very low and can be neglected. This can further be verified by studying the consistent improvement in the gain of DFW slot array antenna described in Table 1.

IV. FABRICATED AND MEASURED OPTIMIZED DIELECTRIC LENS WITH DFW SLOT ARRAY ANTENNA

The optimized graded lens (OGL) presented in Figure 8 as well as an optimized homogeneous lens (OHL) shown in Figure 13, were fabricated for use with the DFW slot array antenna.

Both lenses were fabricated via FDM 3D-printing using polylactic acid (PLA) thermoplastic. PLA has a dielectric constant of up to 2.7 with 100% infill density and a loss tangent of 0.007 at the required frequency band [37], [38].

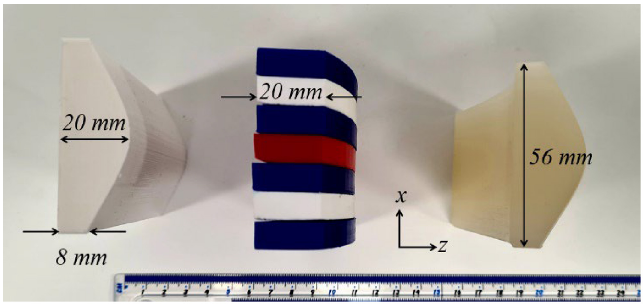

FIGURE 14. 3D printed geometries of the fabricated conventional plano-convex flat lens (CPFL), optimized graded lens (OGL) and optimized homogeneous lens (OHL).

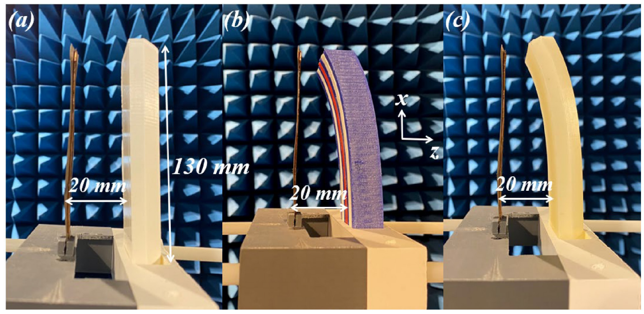

FIGURE 15. (a) Conventional plano-convex flat lens (CPFL); (b) optimized graded lens (OGL); and (c) optimized homogeneous lens (OHL) placed in front of a DFW antenna inside the anechoic chamber.

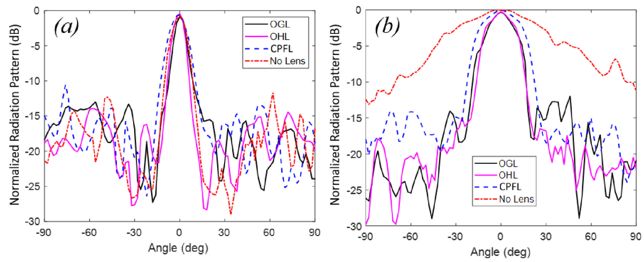

FIGURE 16. Measured normalized radiation patterns at 28 GHz for DFW slot array with optimized graded lens (OGL), optimized homogeneous lens (OHL) and homogeneous conventional plano-convex flat lens (CPFL) in (a) azimuth and (b) elevation planes.

For both the OGL and OHL, triangular infill patterns are used for 3D-printing. The design model for the OHL is presented in Figure 13 and was designed based on the principles stated in [3]. Instead of varying the relative permittivity in the Y-axis, the dielectric thickness was changed to be maximum at the center ($t_0 = 20$ mm) and minimum at the corners ($t_{-Y} = t_{+Y} = 8$ mm), forming a plano-convex lens structure. The curvature in the X-axis was the same as for the OGL. The dielectric lens thickness distribution in the Y-axis is described through the equation,

$$t_y = t_0 - \frac{f_L}{\sqrt{\varepsilon_r}}\left(\frac{1-\cos\delta}{\cos\delta}\right) \tag{6}$$

where, t_y is the thickness of the lens at any point on the y-axis, t_0 is the thickness of the lens at the center ($y = 0$), f_L is the focal length of the lens, ε_r is the relative permittivity of the lens material and δ is the angle between the normal to the antenna and the edge of the lens. The lens width w_h in the Y-axis is calculated from,

$$w_h = 2 f_L \tan\delta \tag{7}$$

A conventional plano-convex flat lens (CPFL) was also 3D-printed with a focal length of 20 mm and is shown in Figure 14. Both, the OHL as well as the CPFL were fabricated with an infill density of 60% which gave the relative permittivity of the material to be $\varepsilon_{60\%} = 2.0$. The different layers of the OGL were created from different infill densities of 100% (for $\varepsilon_0 = 2.7$), 80% (for $\varepsilon_1 = 2.4$), 60% (for $\varepsilon_2 = 2$) and 30% (for $\varepsilon_3 = 1.47$). The three lenses positioned in front of the DFW slot array antenna are shown in Figure 15.

Besides the difference in the physical structures, the two optimized lenses (graded and homogeneous) are electrically similar and should provide similar radiation characteristics. An OHL can be fabricated easily with any generic 3D printer, however the OGL either needs to be fabricated in separate layers or needs specialized software to locally control the 3D-printed infill density in the same print.

The radiation patterns of the three fabricated lenses were measured with the 16-slot DFW slot array antenna in an anechoic chamber and are presented in Figure 16. The patterns were normalized to compare the half power beamwidth of the antenna system. It was found to be reduced from 68° to 32° with the CPFL and to 24° with the optimized lenses in the elevation plane. The HPBW in the azimuth plane stayed almost constant at 10° for the CPFL and reduced to 8° for the optimized lenses.

The measured gain of the antenna system increased from 11.47 dBi to 15.5 dBi at 28 GHz for the CPFL (presenting a 3.8 dB improvement in the gain), which was further improved to 18.95 dBi with the optimized graded or homogeneous lenses, presenting a relative increase of 3.5 dB above the CPFL and gain enhancement compared to no lens of 7.3 dB for the antenna averaged over the whole bandwidth. There was no significant change in the antenna efficiency. This also agrees with the average simulated gain enhancement of 7.6 dB that was presented in Section III-B. The measured and simulated gain comparison for different lens configurations is presented in Figure 17. Note, that the small grooves that can be seen in the fabricated lens in Figure 14 do not significantly affect the lens performance, as they are located near the farthest radiating element on the DFW, where the radiated power is smallest. The measured results are very close to the simulated results, see Figure 17, which provides further evidence that these fabrication imperfections do not have a significant effect.

V. DESIGN GUIDELINES

As described in Section III, variation in the phase delay and amplitude reduction along the radiating elements of a

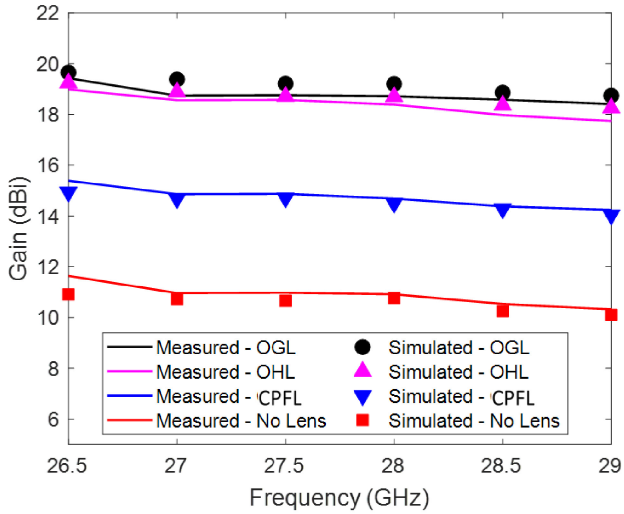

FIGURE 17. Measured and simulated gain of the DFW slot array antenna with homogeneous conventional plano-convex flat lens (CPFL), optimized graded lens (OGL), and optimized homogeneous lens (OHL).

TWA need to be taken into consideration when designing the dielectric lens for a TWA. Results presented in Sections III-C and IV can be replicated for any uniformly or non-uniformly distributed travelling wave antenna with the help of the steps described in this section.

The first step involves the study of phase delay introduced in the EM wave while travelling from the feeding point to each radiating element individually. This can be studied by calculating the equivalent electrical path length and is dependent on the operating frequency and wavelength (or guided wavelength in case of DFWs). Theory of leaky-wave antennas [35], [39] can also be used to calculate the tilt in the wavelet generated by a TWA using eq. (1). Once this tilt has been identified, the conventional flat lens should be placed parallel to the wavelet to reduce distortion in the radiated wave as it passes through the tilted lens.

The second step involves the study of radiation characteristics of each individual radiating element of the TWA. For a uniformly distributed array, the function defined in eq. (3) can be used directly, given that the averaged relative radiated power (ARRP) from each radiating element of the TWA is known, which can be calculated by the multiple-antenna test process described in Section III-B. This ARRP is dependent on the electromagnetic properties of each radiating element and may vary depending on factors such as element spacing, and its dimensions. Therefore, for a generic TWA with non-uniform spacing or varying properties of radiating elements, eq. (3) can be re-written as,

$$P_{rad}(i) = \left[\prod_{i=0}^{n-1}(1-\gamma_i)\right] P_{rad}(1) \quad (8)$$

where, γ_i is the ARRP for the i^{th} radiating element with $\gamma_0 = 0$ and can be calculated individually through the multiple-antenna test process that has been described in Section III-B. The ARRP is found to be constant for uniformly spaced radiating elements, but for non-uniformly spaced elements, the value of ARRP varies with each radiating element. This has been further verified by simulating the DFW slot array antennas with varying element spacing which demonstrated a continuously varying ARRP for each radiating slot. Furthermore, the radiation characteristics of individual elements vary with change in frequency. This is because of variation in electrical path length with frequency, which affects the beam-angle. The ARRP shows slight deflection as we move across different frequency bands, however, this change is very small (within 3%), and hence, has a negligible effect on the performance of the lens with the change in beam-angle or frequency of operation. This can further be verified with the consistent gain enhancement as a function of frequency of the TWA shown in Figure 17.

Equation (3) describes a logarithmically decreasing function, and hence, the general shape of the lens stays the same as presented in Section III-B, with the curvature redefined according to the values of ARRP in eq. (8). Therefore, eq. (8) can be used directly to define the curvature of the optimized dielectric lens for a TWA for both uniformly and non-uniformly distributed radiating elements. This shape of the lens is based on the reducing amplitude of the wavelet radiated by each element, and its shape incorporates the effects of phase delay and amplitude reduction.

This paper presents a complete lens design methodology for optimized lenses. It is worth noting that the design methodology is also applicable to SWAs where each element is identical and receives an equal amount of power. In this case, the ARRP becomes 0 and hence, eq. (8) gives a flat lens, which is identical to a conventional dielectric lens.

VI. FURTHER VERIFICATION OF THE THEORY WITH A MICROSTRIP PERIODIC STUB LOADED LWA

The lens design methodology was further verified by applying it to another TWA, a microstrip line based periodic stub loaded leaky-wave antenna (MPS-LWA). The design was taken from [40], [41] and has been modified to operate at 26 – 29 GHz band and has a frequency based beam-scanning of 15° to 80°. The antenna and its measured S-parameters are shown in Figure 18. An OHL was designed for a focal length, $f_L = 20$ mm using the design guidelines described in Section V and is shown in Figure 19.

The measured normalized radiation patterns for the antenna with and without the optimized lens in the azimuth and elevation planes at 26 – 29 GHz are shown in Figure 20. The HPBW reduced by a factor of 3.2 for all the frequencies. An averaged gain improvement over the frequency band of 7.4 dB was observed with the OHL and is shown in Figure 21. This further confirms the effectiveness of the proposed optimized lens design for any travelling wave antenna. It is noteworthy, that the gain improvement is found to reduce as the beam moves out of the physical area covered

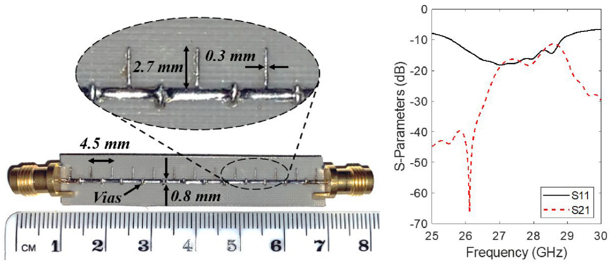

FIGURE 18. Microstrip line based periodic stub loaded leaky-wave antenna and its measured S-parameters.

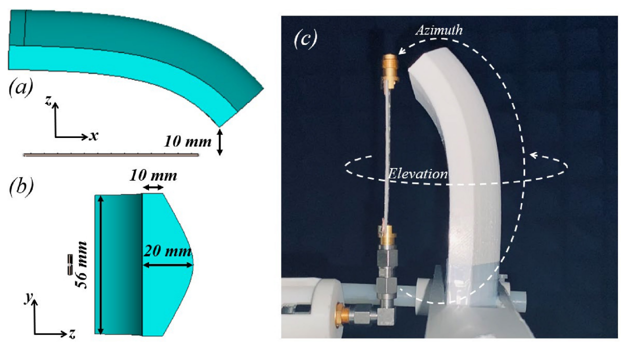

FIGURE 19. CAD model of optimized homogeneous lens in (a) ZX-plane and (b) YZ-plane; (c) fabricated OHL bespoke for the MPS-LWA inside the anechoic chamber.

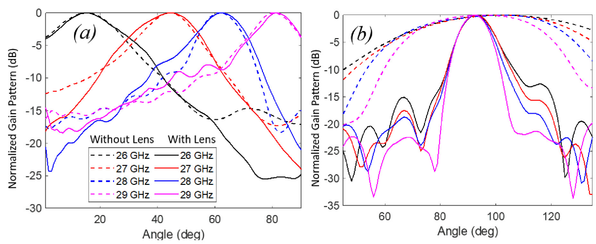

FIGURE 20. Measured normalized radiation patterns for the MPS-LWA without/with the bespoke OHL at 26 – 29 GHz in the (a) azimuth and (b) elevation planes.

by the lens as the lens will only be effective for the beams passing through its cross-section.

VII. CONCLUSION

Lenses are well known antenna components. Although they have been used for TWAs, the gain enhancement is not optimal. This has been highlighted through a comparison of the same lens with both a microstrip patch antenna (representing a standing wave antenna (SWA)) and a dielectric filled waveguide (DFW) slot array antenna (representing a TWA). The comparatively lower gain enhancement recorded for the TWA with the conventional lens, even when tilted appropriately to accommodate the phase delay between radiating slots, demonstrated the need to improve the lens design process for TWAs.

For a 16-slot DFW array antenna, the power radiation profile from each slot and the phase delay between each slot was investigated in detail. Subsequently, equations were derived to transform the conventional graded dielectric lens

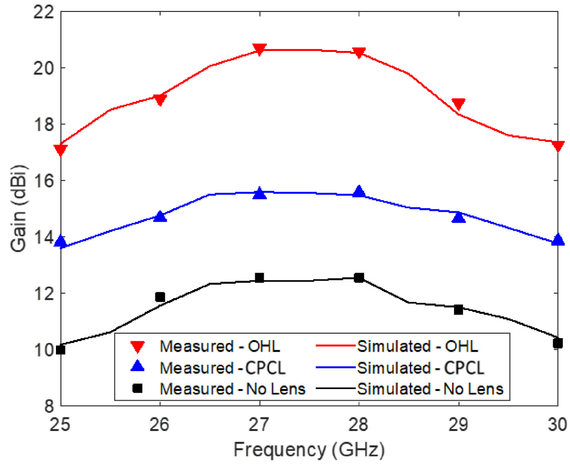

FIGURE 21. Measured and simulated gain for the microstrip periodic stub leaky-wave antenna (MPS-LWA) without and with conventional plano-convex flat lens (CPCL) and optimized homogeneous lens (OHL).

TABLE 2. Gain enhancement of the proposed lens compared with literature for different TWAs.

Ref	Antenna	Lens Type	Freq. Band (GHz)	Avg Gain Increase with lens (dB)
[21]	SIW LWA	Convex Lens	26 – 30	3.2
[22]	SIW LWA	Phase Grating	24 – 27	4.0
[23]	Phased Array	Concave-Convex Lens	6	3.1
[42]	Phased Array	3D U-shaped Phased Shifter	28	3.8
[43]	Spiral Antenna	Hemispherical Lens	25 – 40	4.0
This Work	DFW LWA	OGL and OHL	26 – 30	7.6
This Work	MPS-LWA	OGL and OHL	26 – 29	7.5

from a flat shape to one that has a logarithmic curvature. The theory was verified by fabricating and measuring the radiation patterns of an optimized graded lens (OGL) and an optimized homogenous lens (OHL) with the DFW slot array antenna. The novel optimized lenses enhanced the gain compared to no lens by 7.6 dB (7.5 dB in simulations). The optimized lenses demonstrated a 3.8 dB improvement compared to a plano-convex flat lens (3.5 dB in simulations) and other works compared to literature, see Table 2. This magnitude of gain enhancement is equivalent to that of a conventional dielectric lens when used with a standard SWA. The optimized lens reduced the HPBW accordingly by a factor of approximately three. The total antenna efficiency was found to stay approximately constant within ± 2%.

The proposed lens theory was further verified with an OHL designed for a microstrip periodic stub loaded leaky-wave antenna operating at 26 – 29 GHz. The lens demonstrated a similar average gain enhancement of 7.5 dB over the frequency band with a HPBW reduction by a factor of 3. The cross-polarization results for both the antennas were found to be below −40 dB, and hence are not included in this paper. Finally, a procedure has been proposed that can be followed to optimize dielectric lenses for all TWAs, and the theory is further verified using an MPS-LWA.

REFERENCES

[1] R. Yang, W. Tang, Y. Hao, E. G. Loewen, and E. Popov, "A broadband zone plate lens from transformation optics references and links," *Opt. Exp.*, vol. 19, no. 13, pp. 12348–12355, 2011.

[2] S. Zhang, R. K. Arya, S. Pandey, Y. Vardaxoglou, W. Whittow, and R. Mittra, "3D-printed planar graded index lenses," *IET Microw. Antennas Propag.*, vol. 10, no. 13, pp. 1411–1419, Oct. 2016, doi: 10.1049/iet-map.2016.0013.

[3] S. Zhang, Y. Vardaxoglou, W. Whittow, and R. Mittra, "3D-printed flat lens for microwave applications," in *Proc. Loughborough Antennas Propag. Conf.*, 2015, pp. 1–3, doi: 10.1109/LAPC.2015.7366130.

[4] J. Yi, A. De Lustrac, and S. N. Burokur, "Metamaterial lens for beam steering," in *Proc. 10th Eur. Conf. Antennas Propag. (EuCAP)*, Davos, Switzerland, 2016, pp. 1–4.

[5] S. Jain, M. Abdel-Mageed, and R. Mittra, "Flat-lens design using field transformation and its comparison with those based on transformation optics and ray optics," *IEEE Antennas Wireless Propag. Lett.*, vol. 12, pp. 777–780, 2013, doi: 10.1109/LAWP.2013.2270946.

[6] S. Zhang, R. K. Arya, W. G. Whittow, D. Cadman, R. Mittra, and J. Vardaxoglou, "Ultra-wideband flat metamaterial GRIN lenses assisted with additive manufacturing technique," *IEEE Trans. Antennas Propag.*, vol. 69, no. 7, pp. 3788–3799, Jul. 2021, doi: 10.1109/TAP.2020.3044586.

[7] A. Dadgarpour, B. Zarghooni, B. S. Virdee, and T. A. Denidni, "Beam tilting antenna using integrated metamaterial loading," *IEEE Trans. Antennas Propag.*, vol. 62, no. 5, pp. 2874–2879, May 2014, doi: 10.1109/TAP.2014.2308516.

[8] A. Dadgarpour, B. Zarghooni, B. S. Virdee, and T. A. Denidni, "Improvement of gain and elevation tilt angle using metamaterial loading for millimeter-wave applications," *IEEE Antennas Wireless Propag. Lett.*, vol. 15, pp. 418–420, 2016, doi: 10.1109/LAWP.2015.2449235.

[9] A. Dadgarpour, B. Zarghooni, B. S. Virdee, and T. A. Denidni, "One- and two-dimensional beam-switching antenna for millimeter-wave MIMO applications," *IEEE Trans. Antennas Propag.*, vol. 64, no. 2, pp. 564–573, Feb. 2016, doi: 10.1109/TAP.2015.2508478.

[10] M. Imbert, A. Papio, F. De Flaviis, L. Jofre, and J. Romeu, "Design and performance evaluation of a dielectric flat lens antenna for millimeter-wave applications," *IEEE Antennas Wireless Propag. Lett.*, vol. 14, pp. 342–345, 2015, doi: 10.1109/LAWP.2014.2363596.

[11] M. R. D. Kodnoeih, Y. Letestu, R. Sauleau, E. M. Cruz, and A. Doll, "Compact folded Fresnel zone plate lens antenna for 5G point-to-point communications," in *Proc. IET Conf. Publ.*, 2018, pp. 873–876, doi: 10.1049/cp.2018.0370.

[12] M. K. T. Al-Nuaimi and W. Hong, "Discrete dielectric reflectarray and lens for E-band with different feed," *IEEE Antennas Wireless Propag. Lett.*, vol. 13, pp. 947–950, 2014, doi: 10.1109/LAWP.2014.2313569.

[13] Y. Chen, L. Chen, J.-F. Yu, and X.-W. Shi, "A C-band flat lens antenna with double-ring slot elements," *IEEE Antennas Wireless Propag. Lett.*, vol. 12, pp. 341–344, 2013, doi: 10.1109/LAWP.2013.2247973.

[14] N. T. Nguyen, A. Rolland, A. V. Boriskin, G. Valerio, L. Le Coq, and R. Sauleau, "Size and weight reduction of integrated lens antennas using a cylindrical air cavity," *IEEE Trans. Antennas Propag.*, vol. 60, no. 12, pp. 5993–5998, Dec. 2012, doi: 10.1109/TAP.2012.2208931.

[15] Y. S. Zhang and W. Hong, "A millimeter-wave gain enhanced multi-beam antenna based on a coplanar cylindrical dielectric lens," *IEEE Trans. Antennas Propag.*, vol. 60, no. 7, pp. 3485–3488, Jul. 2012, doi: 10.1109/TAP.2012.2194646.

[16] M. Bosiljevac, M. Casaletti, F. Caminita, Z. Sipus, and S. MacI, "Non-uniform metasurface Luneburg lens antenna design," *IEEE Trans. Antennas Propag.*, vol. 60, no. 9, pp. 4065–4073, Sep. 2012, doi: 10.1109/TAP.2012.2207047.

[17] M. K. T. Al-Nuaimi, W. Hong, and Y. Zhang, "Design of high-directivity compact-size conical horn lens antenna," *IEEE Antennas Wireless Propag. Lett.*, vol. 13, pp. 467–470, 2014, doi: 10.1109/LAWP.2013.2297519.

[18] T. S. Rappaport et al., "Millimeter wave mobile communications for 5G cellular: It will work!" *IEEE Access*, vol. 1, pp. 335–349, 2013, doi: 10.1109/ACCESS.2013.2260813.

[19] Z. Pi and F. Khan, "An introduction to millimeter-wave mobile broadband systems," *IEEE Commun. Mag.*, vol. 49, no. 6, pp. 101–107, Jun. 2011, doi: 10.1109/MCOM.2011.5783993.

[20] O. Quevedo-Teruel, M. Ebrahimpouri, and F. Ghasemifard, "Lens antennas for 5G communications systems," *IEEE Commun. Mag.*, vol. 56, no. 7, pp. 36–41, Jul. 2018, doi: 10.1109/MCOM.2018.1700977.

[21] B. T. Malik, V. Doychinov, S. A. R. Zaidi, I. D. Robertson, and N. Somjit, "Antenna gain enhancement by using low-infill 3D-printed dielectric lens antennas," *IEEE Access*, vol. 7, pp. 102467–102476, 2019, doi: 10.1109/ACCESS.2019.2931772.

[22] W. Cao, W. Hong, Z. N. Chen, B. Zhang, and A. Liu, "Gain enhancement of beam scanning substrate integrated waveguide slot array antennas using a phase-correcting grating cover," *IEEE Trans. Antennas Propag.*, vol. 62, no. 9, pp. 4584–4591, Sep. 2014, doi: 10.1109/TAP.2014.2333058.

[23] Y. Luo and Z. N. Chen, "A scanning angle range enhanced phased array antenna using concave-convex lens," in *Proc. IEEE Int. Conf. Service Oper. Logist. Informat.*, 2018, pp. 17–20, doi: 10.1109/SOLI.2018.8476789.

[24] M. Alonso-Delpino, S. Bosma, C. Jung-Kubiak, G. Chattopadhyay, and N. Llombart, "Wideband multimode leaky-wave feed for scanning lens-phased array at submillimeter wavelengths," *IEEE Trans. THz Sci. Technol.*, vol. 11, no. 2, pp. 205–217, Mar. 2021, doi: 10.1109/TTHZ.2020.3038033.

[25] M. Ebrahimpouri, O. Quevedo-Teruel, M. Ettorre, and A. Grbic, "Ultra-wide band non-dispersive leaky-wave antenna based on glide-symmetric meandered transmission lines," in *Proc. 14th Eur. Conf. Antennas Propag.*, vol. 2, 2020, pp. 2–5, doi: 10.23919/EuCAP48036.2020.9135678.

[26] A. Torki, M. Ebrahimpouri, and O. Quevedo-Teruel, "A planar steerable 60 GHz leaky wave antenna with Luneburg lens feed," in *Proc. Int. Symp. Antennas Propag.*, vol. 2, 2016, pp. 1405–1406, doi: 10.1109/APS.2016.7696409.

[27] M. Ebrahimpouri and O. Quevedo-Teruel, "Bespoke lenses based on quasi-conformal transformation optics technique," *IEEE Trans. Antennas Propag.*, vol. 65, no. 5, pp. 2256–2264, May 2017, doi: 10.1109/TAP.2017.2679494.

[28] M. Ebrahimpouri, O. Zetterstrom, and O. Quevedo-Teruel, "Experimental validation of a bespoke lens for a slot log-spiral feed," *IEEE Antennas Wireless Propag. Lett.*, vol. 19, no. 4, pp. 557–560, Apr. 2020, doi: 10.1109/LAWP.2020.2971852.

[29] Y. J. Cheng et al., "Substrate integrated waveguide (SIW) Rotman lens and its Ka band multibeam array antenna applications," *IEEE Trans. Antennas Propag.*, vol. 56, no. 8, pp. 2504–2513, Aug. 2008.

[30] J. W. Lian, Y. L. Ban, H. Zhu, and Y. J. Guo, "Reduced-sidelobe multibeam array antenna based on SIW Rotman lens," *IEEE Antennas Wireless Propag. Lett.*, vol. 19, no. 1, pp. 188–192, Jan. 2020, doi: 10.1109/LAWP.2019.2957509.

[31] K. Tekkouk, M. Ettorre, L. Le Coq, and R. Sauleau, "Multibeam SIW slotted waveguide antenna system fed by a compact dual-layer Rotman lens," *IEEE Trans. Antennas Propag.*, vol. 64, no. 2, pp. 504–514, Feb. 2016, doi: 10.1109/TAP.2015.2499752.

[32] Y. M. Cheng, P. Chen, W. Hong, T. Djerafi, and K. Wu, "Substrate-integrated-waveguide beamforming networks and multibeam antenna arrays for low-cost satellite and mobile systems," *IEEE Antennas Propag. Mag.*, vol. 53, no. 6, pp. 18–30, Dec. 2011, doi: 10.1109/MAP.2011.6157710.

[33] M. Bozzi, A. Georgiadis, and K. Wu, "Review of substrate-integrated waveguide circuits and antennas," *IET Microw. Antennas Propag.*, vol. 5, no. 8, pp. 909–920, Jun. 2011, doi: 10.1049/iet-map.2010.0463.

[34] L. Yan, W. Hong, G. Hua, J. Chen, K. Wu, and T. J. Cui, “Simulation and experiment on SIW slot array antennas,” *IEEE Microw. Wireless Compon. Lett.*, vol. 14, no. 9, pp. 446–448, Sep. 2004, doi: 10.1109/LMWC.2004.832081.
[35] C. A. Balanis, *Antenna Theory: Analysis and Design*, 3rd ed. New York, NY, USA: Wiley, 2005.
[36] F. Monticone and A. Alù, “Leaky-wave theory, techniques, and applications: From microwaves to visible frequencies,” *Proc. IEEE*, vol. 103, no. 5, pp. 793–821, May 2015, doi: 10.1109/JPROC.2015.2399419.
[37] C. K. Lee et al., “Evaluation of microwave characterization methods for additively manufactured materials,” *Designs*, vol. 3, no. 4, pp. 1–17, 2019, doi: 10.3390/designs3040047.
[38] T. Whittaker, S. Zhang, C. Stevens, A. Powell, J. C. Vardaxolgou, and W. G. Whittow, “3D printing materials and techniques for antennas and metamaterials,” *IEEE Antennas Propag. Mag.*, early access, Dec. 26, 2022, doi: 10.1109/MAP.2022.3229298.
[39] R. S. Elliott, *Antenna Theory and Design Revised Edition* (Series on Electromagnetic Wave Theory). New York, NY, USA: IEEE Press, 2003.
[40] Y. L. Lyu, F. Y. Meng, G. H. Yang, Q. Wu, and K. Wu, “Leaky-wave antenna with alternately loaded complementary radiation elements,” *IEEE Antennas Wireless Propag. Lett.*, vol. 17, no. 4, pp. 679–683, Apr. 2018, doi: 10.1109/LAWP.2018.2811726.
[41] S. Paulotto, P. Baccarelli, F. Frezza, and D. R. Jackson, “A novel technique for open-stopband suppression in 1-D periodic printed leaky-wave antennas,” *IEEE Trans. Antennas Propag.*, vol. 57, no. 7, pp. 1894–1906, Jul. 2009, doi: 10.1109/TAP.2009.2019900.
[42] E. Kim, S. T. Ko, Y. J. Lee, and J. Oh, “Millimeter-wave tiny lens antenna employing U-shaped filter arrays for 5G,” *IEEE Antennas Wirelesss Propag. Lett.*, vol. 17, no. 5, pp. 845–848, May 2018, doi: 10.1109/LAWP.2018.2819022.
[43] A. Garufo, N. Llombart, and A. Neto, “Radiation of logarithmic spiral antennas in the presence of dense dielectric lenses,” *IEEE Trans. Antennas Propag.*, vol. 64, no. 10, pp. 4168–4177, Oct. 2016, doi: 10.1109/TAP.2016.2593744.

AAKASH BANSAL (Member, IEEE) received the Bachelor of Technology (B.Tech.) degree in electronics and communication engineering from Guru Gobind Singh Indraprastha University, Delhi, India, in 2017 and the Ph.D. degree in electronics, electrical and systems engineering from Loughborough University, U.K., in 2022. He worked as a Research Associate with CSIR—Central Electronics Engineering Research Institute, Pilani, India, from 2017 to 2019. He is currently working as a Postdoctoral Research Associate with the Wolfson School of Mechanical, Electrical, and Manufacturing Engineering, Loughborough University. His research is focused on active millimeter-wave beam-steering antenna array systems for 5G and beyond. His research interests include beamforming, beam-steering antennas, metamaterials, dielectric lenses, antenna arrays, and leaky-wave antennas. He has received IEEE Richard E. Merwin Student Scholarship in 2016, Loughborough University’s Sir Robert Martin University Prize in 2020, and Loughborough University’s Doctoral Researcher’s Presidential Award in 2022.

CHINTHANA J. PANAGAMUWA received the Master of Engineering (M.Eng.) degree in electronics and electrical engineering and the Ph.D. degree in electronics and electrical engineering from Loughborough University, U.K., in 2000 and 2005, respectively, where he is a Senior Lecturer in Wireless Communications with the Wolfson School of Mechanical, Electrical, and Manufacturing Engineering. His research interests include optically activated semiconductor switches for microwave circuits, devices, and antennas. He also conducts research on specific absorption rates due to mobile communications devices and in-body antennas. He was previously the Coordinating Chair of the Loughborough Antennas and Propagation Conference series since 2011.

WILLIAM G. WHITTOW AFWES SFHEA SMIEEE (Senior Member, IEEE) received the B.Sc. degree in physics and the Ph.D. degree in computational electromagnetics from the University of Sheffield, Sheffield, U.K., in 2000 and 2004, respectively. From 2004 to 2012, he was a Research Associate with Loughborough University, Loughborough, U.K, where he became a Lecturer with the Wolfson School of Mechanical, Electrical and Manufacturing Engineering in 2012. He became a Senior Lecturer in 2014, a Reader (Associate Professor) in 2018, and a Professor of Radiofrequency Materials in 2020. He leads the Wireless Communications Research Group and the Director of the Connected Infrastructure Research Priority. He is a Named Investigator on research grants totaling in excess of £14m. He has authored more than 280 peer-reviewed journal and conference papers in topics related to *metamaterials*, metasurfaces, synthetic and heterogeneous dielectrics, dielectric measurements, 3D-printing, wearable antennas and phantoms, specific absorption rate, embroidered antennas, inkjet printing, and RFID tags. From 2007 to 2011, he was the Coordinating Chair of the Loughborough Antennas and Propagation Conference. In 2017, he won the Women in Engineering Society (WES) Men as Allies Award. He has served as an Associate Editor of *IET’s Electronics Letters* and also *Microwaves, Antennas and Propagation*. He serves on the technical programme committees of several IEEE international conferences. He has been asked to give more than 30 invited conference presentations; a 4-day invited workshop on Bioelectromagnetics and teaches about dielectric measurements at the European School of Antennas. He is the Inaugural Male Associate Fellow of WES. He is a Senior Fellow of the Higher Education Academy. More than 95 of his academic journal papers can be freely downloaded here: http://publications.lboro.ac.uk/publications/all/collated/elwgw.html. A video of his research about 3D printed RF devices can be found here: https://www.youtube.com/watch?v=d5ko7WhHUHA.